Geology, Geophysics & Environment 2024, vol. 50 (3): 275–293

Geothermal energy potential of Main Dolomite formation in SW Poland

Małgorzata Słota-Valim[1], Anita Lis-Śledziona[2], Tomasz Topór[3]

[1] *Oil and Gas Institute-National Research Institute, Krakow, Poland, e-mail: slota-valim@inig.pl (corresponding author), ORCID ID: 0000-0002-5915-7614*
[2] *Oil and Gas Institute-National Research Institute, Krakow, Poland, e-mail: lis-sledziona@inig.pl, ORCID ID: 0000-0003-3067-3014*
[3] *Oil and Gas Institute-National Research Institute, Krakow, Poland, e-mail: topor@inig.pl, ORCID ID: 0000-0002-5306-4636*

Received: 23 May 2024; accepted: 17 June 2024; first published online: 30 September 2024

Abstract: This paper evaluates the geothermal potential of the Main Dolomite formation in an oil and gas field on the Fore-Sudetic Monocline (SW, Poland). The reservoir characterization included a well-logging interpretation and developed 3D petrophysical and temperature models that provided information on storage potential, transport properties, and temperature conditions in the analyzed carbonate formation. Geothermal energy potential was assessed using heat in place (HIP) and recoverable heat (Hrec) parameters for water and CO_2 systems, considering a 50-year plant lifespan. Petrophysical and temperature data classify reservoirs using unsupervised machine learning, identifying zones with high and low geothermal potential, noting a strong limestone and dolomite dichotomy. Dolomite horizon shows more promising reservoir quality with mean porosity and permeability of 0.045 and 0.4 mD, respectively, however, its mean thickness reaches 11.58 m at maximum. The calculated Hrec for a 50-year lifetime of a geothermal system varies across dolomite horizon. In the most promising areas of NNW, WSW, and E parts, the values of Hrec are 8.19, 3.47, and 1.34 MW for water, respectively, and 0.69, 0.29, and 0.11 MW for CO_2 as working fluids. Remarkably, the energy locked in the NNW zone constitutes nearly 21% of the total geothermal energy potential within the entire dolomite horizons of the study area. The geothermal resources for the most perspective location within the dolomite horizon were estimated at 12.99 and 1.09 MW levels, using water and CO_2 as working fluids, respectively, assuming 50 years of the project's lifetime.

Keywords: geothermal resources, geothermal system modelling, 3D geological modelling, machine learning

INTRODUCTION

The growing demand for energy and the need for a transition from fossil fuel sources towards alternative energy sources are leading to the intensive development of green energy technologies. This includes energy from the Earth's heat, known as geothermal energy.

The share of geothermal energy in the structure of renewable sources in the studied areas is insignificant, reaching 2.8% in Poland (geothermal and heat pumps), with the share of renewable energy sources in the Polish energy mix at 20.6.%, where coal is the leader (69%), and gas takes a share of 6.5% in the structure of energy sources in this country (GUS 2023).

These numbers show the urgent necessity for developing technologies in geothermal energy, focusing on resource assessment, development, and utilization in Poland.

The history of recognizing geothermal waters in Poland dates back to the 13th century, when

the Orders of St. John founded the first health resort utilizing balneotherapy in Cieplice (PIG-PIB 2024). It was only later, at the beginning of the 1990s, that efforts were made to use geothermal energy in heating (Noga et al. 2013). The recognition of the potential for converting geothermal energy into electricity began with research projects initiated in 2010–2013. These projects identified the locations of geothermal systems that require stimulation, known as Enhanced Geothermal Systems (EGS), in Poland (Górecki et al. 2015, Sowiżdżał et al. 2016, Sowiżdżał 2018). Additionally, an atlas for using thermal waters in combined electricity and heat production in binary systems in Poland was developed (Bujakowski & Tomaszewska red. 2014). The most recent results from the EnerGizer project provided a multi-aspect consideration for the development of EGS with CO_2 in Poland in terms of petrophysical evaluation (Sowiżdżał et al. 2022b), techno-economic assessment (Chomać-Pierzecka et al. 2022, Tagliaferri et al. 2022), and social aspects (Wachowicz-Pyzik et al. 2024).

Various geological and engineering classifications of geothermal systems are found in the literature. Geological classifications are based on tectonic location, geological conditions, and how these systems were formed (Moeck 2014, Syukri et al. 2018). On the other hand, engineering classifications differentiate between geothermal systems based on the dominant heat exchange mechanism, their performance during well testing, and their response to long-term production. Understanding the type of geothermal system is essential for the success of any commercial investment.

To achieve effective commercial energy production from a geothermal system, specific criteria must be met. These include a high reservoir rock temperature, a sufficiently large reservoir capacity defined by the reservoir rock volume and its porosity, and the permeability of the rock to allow the flow of geothermal energy to production wells (Huang et al. 2021, 2022, Sowiżdżał et al. 2022a).

Characterizing the reservoir rock in geothermal systems is fundamental for efficient heat extraction and serves as the basis for numerical simulations of the system's operation. Reliable characteristics of the potential geothermal reservoir system help minimize many risks, especially the likelihood of not finding geothermal energy resources in commercial quantities (Okoroafor et al. 2022, Sowiżdżał et al. 2022a).

An essential aspect of optimizing geothermal energy extraction is the placement of wells in productive high-temperature zones with favorable petrophysical characteristics, specific reservoir potential, and flow parameters for the heat carrier. Methods for the quantitative and qualitative characterization of petrophysical properties and thermal conditions in 3D space involve physics-based numerical modeling using a wide range of data, including laboratory data, wellbore geophysics, seismic data, and complementary geological information.

The combination of 3D numerical modelling, providing the petrothermal characterization of the investigated reservoir, with machine learning classification methods demonstrated feasibility in rock differentiation and proved helpful in identifying sweet spots (Li and Sun, 2016) and more advantageous zones for the optimal location of geothermal wells, working as production-injection doublets (Topór et al. 2023).

This paper presents the results of a reservoir rock characterization in the Main Dolomite formation (Zechstein) in the oil and gas field located on Fore-Sudetic Monocline (SW, Poland) to assess its geothermal potential. The reservoir characterization process included well-logging interpretation supporting developed 3D petrophysical and temperature models that provided information on temperature conditions, storage potential, and transport properties in analyzed carbonate formation. The geothermal energy resources were estimated by defining the heat in place (HIP) and recoverable heat (Hrec) parameters for the water and CO_2 systems. Together with petrophysical and temperature characteristics, these parameters were used to classify the reservoir using generalized fuzzy c-means (gFCM) methods to determine zones with high and low potential for geothermal energy extraction. Hrec resources for water and CO_2 as energy carriers for the most prospective zone were calculated considering the 50-year lifetime of the power plant. The assessment of the area's prospects also considered the presence of existing infrastructure in the form of boreholes.

GEOLOGICAL SETTING

The research area is located to the northeast of the Pogorzela High, which constitutes the southeastern part of the Wolsztyn High in the Permian-Mesozoic substratum of the northern part of Fore-Sudetic Monocline (Kwolek & Mikołajewski 2007). The rock formation considered as a potential geothermal reservoir is developed in the Main Dolomite (Ca2), belonging to the Stassfurt cyclothem, one of the four cyclothems – PZ1 to PZ4 – recognized in the Polish part of the Permian Basin, deposited as a result of successive transgressions of the Zechstein Sea (Fig. 1A) (Wagner 1994, Peryt 2010).

The Zechstein Sea entered an area with varied morphological deposition surfaces in the analyzed part of the Southern Permian Basin. Significant elevation variations contributed to the basin's division into shallow and deeper sea zones. Elevated areas formed platforms and microplatforms of sulfate sediments of the Werra cyclothem, covered with platform-type Main Dolomite deposits resulting from a transgressive cycle during the Stassfurt cyclothem (Czekański et al. 2010). Sedimentological studies of the Main Dolomite revealed the existence of various sedimentary environments resulting from significant bathymetric differences (Peryt & Dyjaczyński 1991, Protas & Wojtkowiak 2000, Jaworowski & Mikołajewski 2007). These include platform and microplatform zones (including a barrier and platform plain), slopes and the base of the slope, and deep-water zones (Mikołajewski & Słowakiewicz 2008, Jaworowski & Mikołajewski 2007).

In the study area, dolomite deposits were formed in the shallower zone of the basin plain, occurring on the outskirts and in bays in the conditions of a low-energy sedimentation environment, in which they reached a thickness of just over 10 m (Zych 2009).

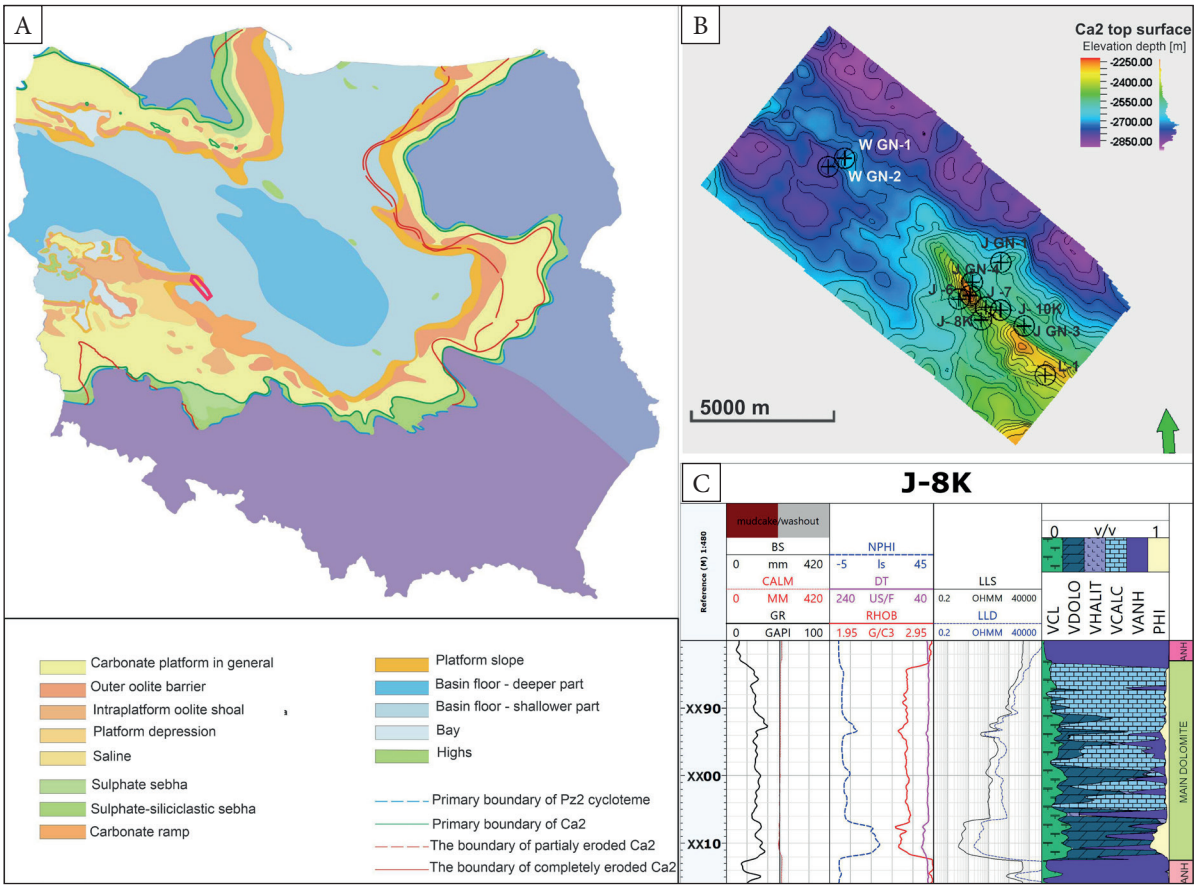

Fig. 1. *Location of the research area marked with a red rectangle on the map of the Main Dolomite distribution in Poland (Wagner et al. 2000, modified) (A), part of the structural map of the top of the Main Dolomite in study area (B) well-log input data recorded in J-8K borehole used for interpretation, and resulting lithological profile (C)*

Only in the profile of three boreholes were larger thicknesses of Ca2 Main Dolomite found, which could sediment in the conditions of gentle slopes of platforms with higher sediment deposition energy and led to thicker Ca2 carbonate deposits above 18 m in the J-6 well, locally reaching up to 29 m in the J-8K well.

Development of the Main Dolomite

The sediments of the Main Dolomite Ca2 in the study area were deposited in a platform ramp environment. The lack of microfacial variability may suggest that these are basin-plain sediments formed in shallow water conditions in low-energy zones. Low-energy zones are associated with platform depressions, with abundant oncolites and bioclasts. The mudstones are microfacially carbonate with sporadic organic matter and coarser grain material associated with distal parts of turbidite flows (Jaworowski & Mikołajewski 2007). Mudstones, due to the presence of organic matter, may represent source rocks.

Microscopic observations conducted on thin sections from boreholes J-8K and J-10K indicated the presence of a simple microfacies assemblage in the Ca2 Main Dolomite profile. The reservoir is developed as mudstones characterized by monotonous bedding with silt-clayey streaks and tectonically originated fractures filled with carbonates and anhydrite. A thin level, possibly packstones with relics of algal structures and strongly impregnated with anhydrite, is observed in the lower part. Preserved remnants of original algal structures suggest a significant contribution of these organisms in the formation of Ca2 Main Dolomite deposits (Peryt & Mikołajewski 1997).

The Ca2 reservoir displays a dual nature, with hard, low-porosity limestones dominating the upper part and dolomites with porosities reaching several percent in the lower part of the Main Dolomite profile. The upper limestone can be streaked with clay-iron substances or impregnated with anhydrite and bituminous material (algae). In contrast, the lower dolomite or dolomitic limestone can be locally impregnated with anhydrite and relics of algal structures.

The Ca2 profile is heavily fractured, with vertical fissures running at an angle of 45°. Most of the fractures are filled with carbonates and anhydrite. Among the numerous microstylolite occurrences, microstylolites of tectonic origin are observed (Peryt & Mikołajewski 1997).

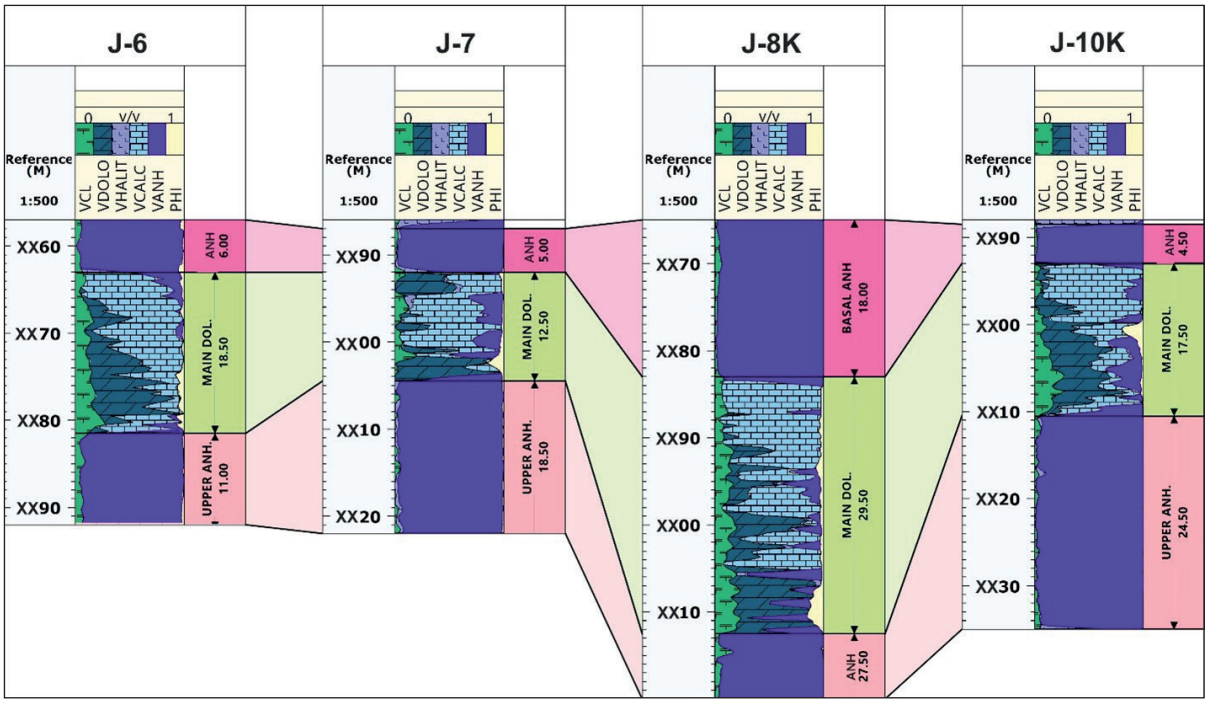

Fig. 2. *Multi-well correlation of the Main Dolomite level in the interpreted wells*

The Main Dolomite reservoir level, both in the upper and lower parts, is isolated by a layer of polycrystalline anhydrite with a chaotic structure (Basal Anhydrite, Main Anhydrite).

Figure 2 presents the multi-well correlation in the interpreted wells through the Main Dolomite level.

METHODOLOGY

To meet the study objectives, petrophysical and temperature conditions were characterized based on well-log data interpretation, which supported the development of 3D parametric models of the analyzed reservoir. For 1D and 3D models construction, a range of data was used, including 3D seismic data and the results of laboratory measurements performed on the core samples from J-6, J-7, J-8K, and J-10K boreholes, along with a set of well log data from these wells.

The sources of information about the structure and reservoir rock parameters in the Main Dolomite (Ca2) were:

- borehole data provided by the reservoir operator, PGNiG Orlen S.A.: J-6, J-7, J-8K, and J-10K, as well as stratigraphic data for other boreholes located in the research area and available in the Central Geological Database (CBDG n.d.): W GN-1, W GN-2, J GN-1, J GN-2, J GN-3, J GN-4, J GN-5, and L-1;
- a 3D seismic image of the reservoir area in the depth domain provided by field operator, PGNiG Orlen S.A.

Based on the developed parametric models, maps of average parameters were prepared which helped to determine the location of zones with favorable geothermal conditions of the analyzed Main Dolomite Ca2 using the generalized fuzzy c-means (gFCM).

Interpretation of well log data

Well-log data interpretation of Ca2 formation aimed to characterize reservoir properties. The petrophysical reservoir parameters were calculated in four wells: J-6, J-7, J-8K, and J-10K.

A comprehensive petrophysical analysis was performed using the Quanti Elan (QE) module within the Techlog software by Schlumberger. During interpretation, the following parameters were calculated: clay volume (VCL), calcite volume (VCALC), dolomite volume (VDOLO), anhydrite volume (VANH), halite volume (VHALIT), and core calibrated porosity (PHI). Water saturation (SW) and irreducible water content (SWI) were also calculated.

During the interpretation, the following model was adopted:

$$\text{VCL} + \text{VCALC} + \text{VDOLO} + \text{VHALIT} + \\ + \text{VANH} + \text{PHI}.$$

The QE module was used for lithological and porosity analysis with deterministic linear inversion. This module calculates mineral volumes using a least-squares method based on the final geological model. Synthetic input curves are generated based on the final geological model and compared with measured well logs. The difference between the calculated synthetic logs and the measured ones is an error of the evaluated model.

The input data in most wells included natural gamma ray (GR), compressional slowness (DT), neutron porosity (NPHI), bulk density (RHOB), resistivity of the uninvaded zone, resistivity of the flushed zone, and in some wells also, the photoelectric factor (PE), concentrations of thorium (THOR), uranium (URAN), and potassium (POTA) were also available.

Clay volume (VCL) was initially estimated using a linear formula. The values of GRmatrix ranged from 5–10 API for limestones and 5–7 API for anhydrites, while the values of GR of shale were assumed to be in the range of 110–150 API.

$$\text{VCL} = \frac{\text{GR} - \text{GRmatrix}}{\text{GRshale} - \text{GRmatrix}} \tag{1}$$

Porosity is a parameter that determines the storage capacity of a rock. It provides information about empty spaces within the rock, which can vary in size and shape. Important factors influencing the properties of the pore space include mineral composition, structure, texture, size, arrangement, shape, degree of grain rounding, sorting, and the quantity and type of cementing material. An increase in cementing material typically leads to a decrease in effective porosity.

Three basic well logs were used for preliminary porosity calculations: compressional slowness (DT), neutron porosity (NPHI), and bulk density

(RHOB). Two methods were employed: neutron-density (PHIND) based on NPHI and RHOB measurements and neutron sonic (PHI_NS) utilizing NPHI and DT measurements.

Calculated values of effective porosity were calibrated with core porosity. Initially, the calculated values of VCL and PHI were input into the QE module with a specified level of uncertainty. Temperature (FTEMP) and hydrostatic pressure (HYDROPRESSURE) were also computed in the profile of each well and calibrated with the measured values of pressure and temperature available in the borehole documentations of J-7, J-8K, and J-10K wells.

Permeability determines the rate of fluid movement through the pore and fracture network within the rock structure (Jarzyna et al. 1999). This parameter depends on pore size, diameter, shape, and the degree of hydraulic connectivity, all of which affect the flow of fluids or gases within rocks. In the calculations of irreducible water content and permeability, equations developed by Zawisza and Nowak (2012) for the Grotów and Lubiatów regions (close to the study area) were applied (Equations (2)–(5)), with slight modifications to *a* and *b* coefficients which are calibration exponents. Calculated permeability (Perm) was calibrated with laboratory values of permeability measured on the core samples. Laboratory measurements of porosity and permeability within the Main Dolomite reservoir level were also compared on the cross plots (Fig. 3). However, the relatively small amount of laboratory measurements and the influence of fractures did not establish a reliable relationship between permeability and porosity. A better calibration was achieved using Zawisza's models, which consider not only porosity but also the effect of irreducible water content.

Grotów area:

$$SWI = (VCL + 0.005)^{0.1} \cdot (1 - PHI)^{14.5} \quad (2)$$

$$PERM = 66 \cdot PHI^2 \cdot (1 - SWI)^2 \quad (3)$$

Lubiatów area:

$$SWI = (VCL + 0.005)^{0.1} \cdot (1 - PHI)^{14.5} \quad (4)$$

$$PERM = 2465 \cdot PHI^2 \cdot (1 - SWI)^2 \quad (5)$$

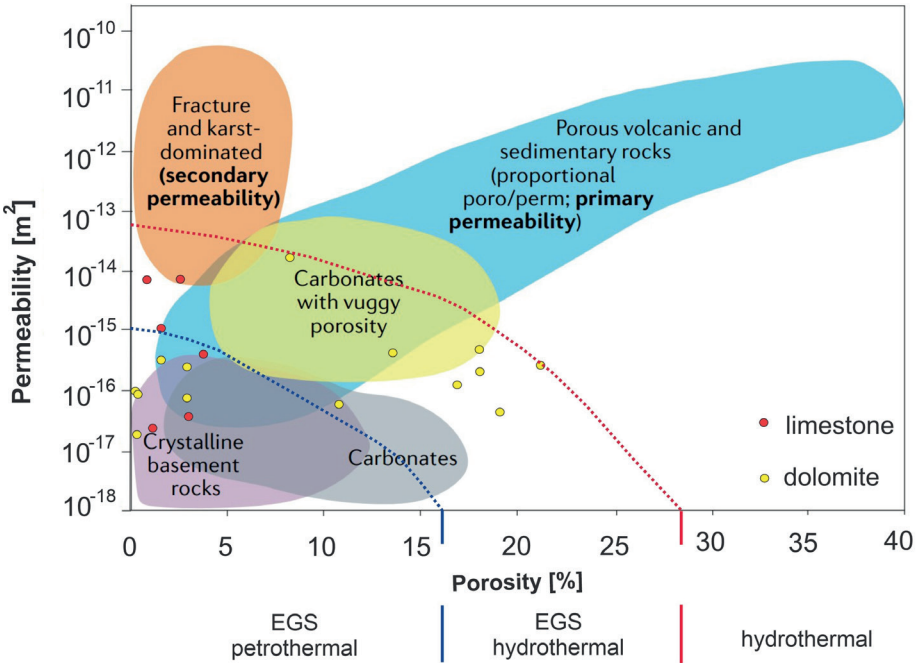

Fig. 3. *The relationship between porosity and permeability measured on core samples from the Ca2 Main Dolomite interval against the sketch with the classification of geothermal systems based on petrophysical parameters in the background (Jolie et al. 2021, modified)*

Water saturation is a key and final parameter in interpreting petrophysical data because it allows for defining prospective hydrocarbon saturated zones. For geothermal energy resources, assessment of water saturation is critical, as water is the energy carrier in a water-based system. In the case of oil and gas reservoirs in the development stage, the water saturation parameter will change dynamically, increasing its value along with hydrocarbon production (Khasani et al. 2004, Huang et al. 2022). Water saturation analyses were preceded by calculating the resistivity of the formation water. The water salinity was assumed based on the data available in the documentation of the individual wells. The water saturation coefficient was calculated according to Archie's equation (1942) (6).

$$\mathrm{SW}^n = \frac{a \cdot R_w}{\mathrm{PHI}^m \cdot R_t} \tag{6}$$

where SW represents the water saturation, R_t represents the true formation resistivity (resistivity of the uninvaded zone), R_w is the resistivity of formation water, PHI stands for effective porosity, m is the cementation exponent, and n – saturation exponent.

For further modeling, a simple lithofacial classification was conducted. As a result, two lithotypes were defined: hard, non-porous limestones occurring at the top of the reservoir and porous dolomites and dolomitic limestones occurring at the bottom of the reservoir zone.

Figure 4 presents measured well-log data and the interpretation results in the well J-8K.

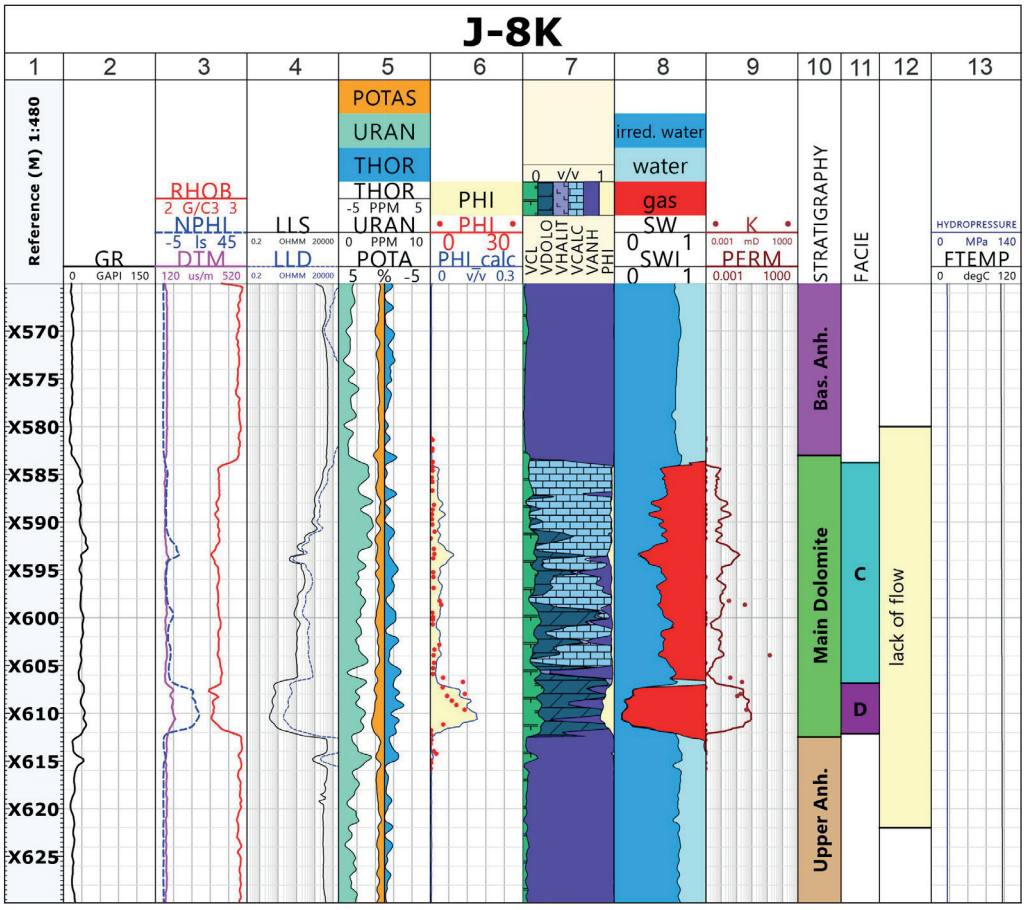

Fig. 4. *Measured well logs and interpretation results in the J-8K well. Track: 1 – depth (MD), 2 – gamma ray (GR), 3 – compressional slowness (DT), neutron porosity (NPHI), and bulk density (RHOB), 4 – resistivity of uninvaded zone (LLD) and flushed zone (LLS), 5 – thorium (THOR), potassium (POTA), and uranium (URAN) content, 6 – calculated porosity (PHI_calc) and measured porosity (red points), 7 – lithology (VCL – shale volume, VDOLO – dolomite volume, VCALC – calcite volume, VANH – anhydrite volume, VHALIT – halite volume, PHI – porosity), 8 – irreducible water content (SWI) and water saturation (SW), 9 – calculated permeability (PERM) and measured permeability (K), 10 – stratigraphy, 11 – lithofacies (C – limestone, D – dolomite), 12 – well test results, 13 – formation temperature (FTEMP), and hydrostatic pressure (HYDROPRESSURE) values*

The average values of reservoir parameters within the Ca2 formation are as follows: clay volume 11.1%, porosity (core calibrated) 3.6%, the geometric mean of absolute permeability 0.005 mD and median 0.006 mD, and water saturation coefficient 59%. Statistical characteristics of clay volume, porosity, permeability, and water saturation coefficient in the analyzed four wells within the Ca2 reservoir are depicted in Table 1.

Table 1
Statistics of the reservoir parameters in the analyzed 4 wells: J-6, J-7, J-8K, J-10K within Ca2 reservoir level

Statistics	VCL [v/v]	PHI [v/v]	PERM [mD]	SW [v/v]
Mean	0.112	0.036	0.005	0.592
Median	0.111	0.026	0.007	0.543
Min. value	0	0	0	0.082
Max. value	0.278	0.201	1.751	1.000

Development of a 3D structural and parametric models

The structural model of the study area was developed based on a dataset that includes the seismic image and stratigraphic markers from boreholes. During the model construction stage, fault zones were considered as they may play a critical role in the geothermal water flow simulation (Kaminskaite et al. 2021, Ahrens et al. 2022). Since the Main Dolomite Ca2 exhibits a clear dichotomy in the profiles of all analyzed wellbores, the model delineated a layer of limestones and dolomitic limestones in the upper part with a higher thickness averaging at 9.86 m and a layer of calcareous dolomites in the lower part with an average thickness of 6.85 m. The limestone horizon exhibits significantly poorer reservoir transport properties (Fig. 5).

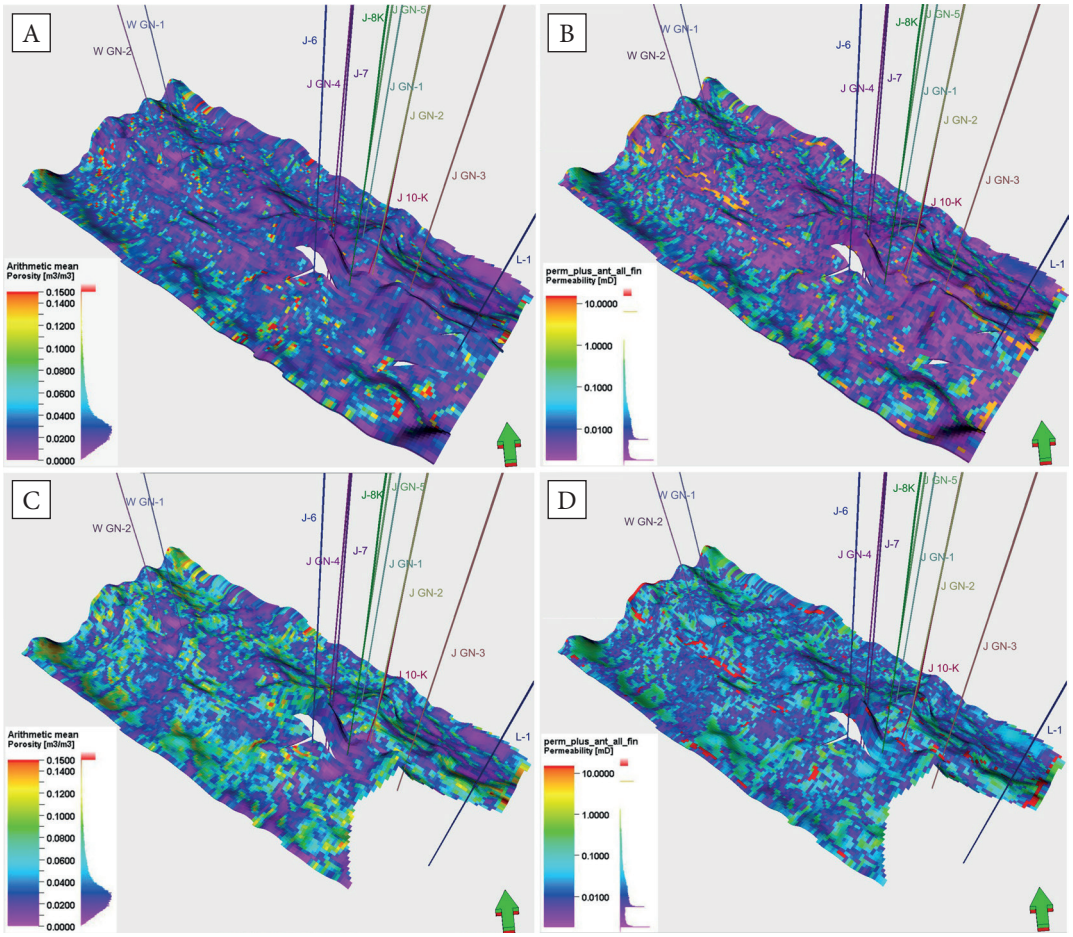

Fig. 5. *Visualization of the spatial porosity and permeability models in the limestone horizon in the upper part of the Main Dolomite (Ca2) profile (A, B) and dolomite horizon in the lower part of the Main Dolomite (Ca2) profile (C, D)*

3D models for porosity, permeability, and temperature

Information about the reservoir rock quality for the geothermal potential assessment was obtained from well-log data calibrated with laboratory core analysis results in wells J-6, J-7, J-8K, and J-10K. Additionally, to develop 3D parametric models, an amplitude cube from the 3D seismic image was used to reduce the uncertainty of parameter distributions, especially in the horizontal direction.

Due to the observed lower variability of petrophysical parameters within the identified lithotypes, including limestones and dolomitic limestones in the upper part and calcareous dolomites in the lower part of the Ca2 profile, effective porosity and permeability models were developed individually for each lithotype.

3D porosity model. The data used for 3D porosity model were averaged to match the vertical resolution of the block model through an upscaling procedure. Subsequently, the geostatistical data analysis on the input data was carried out. The data was appropriately transformed at this stage, and variogram parameters were determined individually for limestones and dolomites. Semivariogram parameters, which govern the interpolation of input data within the spatial grid of the 3D model, were determined during statistical analysis. A stochastic algorithm, Gaussian random function simulation, was used to model the spatial distribution of porosity. The modeling process was repeated 15 times, resulting in 15 equally probable realizations. The final representation of the modeled porosity parameter distribution was obtained through arithmetic averaging the generated realizations.

3D permeability model. The spatial permeability model was based on interpreted permeability from well-logs profiles. Similarly to porosity, the input data were averaged through an upscaling procedure and then subjected to geostatistical analysis. Calculations of the 3D distribution of the permeability parameter in the block model were performed individually for each lithofacial unit using the appropriate set of control parameters determined during the statistical analysis of input data.

Due to the observed positive correlation between effective porosity and the modeled permeability with a correlation coefficient above 0.9 for both lithotypes (Table 2), this relationship was utilized to calculate the spatial distribution of permeability.

We used the Gaussian random function simulation algorithm with an active co-kriging option that treated porosity as a controlling element in the computational process to calculate spatial permeability distribution.

The modeling process was repeated 15 times, resulting in 15 realizations with the same probability. The final distribution of the modeled permeability was obtained through the arithmetic averaging of these 15 realizations. The final permeability distribution was then modified by increasing the permeability parameter in zones suspected of containing fractures. Potential discontinuities were distributed using a structural method applied to 3D seismic data, automatically tracking faults and fractures within the seismic volume – ant-track (Hafiz et al. 2022). The parameters of the ant-track method were configured to detect more significant discontinuities. Because the discontinuities tracked by the ant-track algorithm aligned with the trend interpreted on an archival structural map (Pikulski 1997), they were considered reliable, and modifications to permeability were made in these zones. In the areas defined as discontinuous, permeability values were assigned at levels of those measured in limestone and dolomite samples with fractures, respectively. The laboratory measurements show that for some samples with low porosity of around 2%, anomalously high permeabilities were recorded at 6.245 mD for limestone and 14.958 mD for dolomite.

The developed spatial permeability model is presented graphically in Figures 5B and D for limestones and dolomites separately, together with the distribution of the values in the form of histograms in the upper left corner of each figure.

Table 2

The relationship between porosity and permeability developed in the limestone and dolomite horizons in well J-7 (y – permeability, x – porosity)

Lithotype	Model porosity vs. permeability	Correlation coefficient *R*
Limestone	$y = -0.00324637 + 0.269155x + 7.72424x^2$	0.91
Dolomite	$y = 0.0637985 - 3.47108x + 51.6707x^2$	0.99

The histograms depicting the permeability distributions for the identified lithotypes indicate better transport conditions in the dolomite horizon expressed with significantly higher average permeability value in dolomites (0.4 mD) compared to limestones (0.2 mD) (Table 3), which is directly related to the higher porosity in dolomites.

The temperature distributions were developed, similarly to the petrophysical parameters, for the geometry determined by the 3D structural model of the Ca2 Main Dolomite level. Spatial temperature distributions were calculated based on the computed temperatures, using the temperature gradient method in the J-6, J-7, J-8K, and J-10K well profiles and calibrated with measured temperature values in the J-7 and J-8K wells. 3D temperature models were developed using an algorithm that honors the geothermal gradient in the vertical direction. Temperatures recorded in the boreholes are consistent with the range of temperatures modeled in the study area (Hajto 2006).

Identification of high geothermal potential zones

The geothermal resources in the examined reservoir rocks in the Main Dolomite interval were estimated using the heat in place (HIP) approach introduced in the 1970s (Nathenson 1975, Muffler & Cataldi 1977) and modified in more recent research. The HIP parameter takes into account rock volume, average temperature of the reservoir rock, reference temperature, and reservoir rock-fluid properties, including density, porosity, and specific heat of the geothermal system components (Topór et al. 2023).

The HIP in the analyzed Main Dolomite (Ca2) reservoir rock was estimated using the following formula (Piris et al. 2021):

$$\mathrm{HIP} = V \cdot \left[\varphi \cdot \rho_F \cdot C_F + \left(1 - \varphi\right) \cdot \rho_R \cdot C_R \right] \cdot \left(T_r - T_0\right) \quad (7)$$

where V stands for the rock volume [m³], φ is the effective porosity, ρ_F and ρ_R are the working fluid and rock matrix densities, respectively [kg/m³], C_F and C_R are the working fluid and rock matrix heat capacities respectively [kJ/(m³ · °C)], T_r is the reservoir temperature, and T_0 is the average annual surface temperature [°C].

Calculated heat in place (HIP) allows to determine recoverable heat (Hrec), accounting for the thermal power that can be produced in a specified lifetime of the geothermal system (Piris et al. 2021):

$$\mathrm{Hrec} = \frac{\left(\mathrm{HIP} \cdot C_e \cdot R_g\right)}{\left(T_{\mathrm{life}} \cdot P_f\right)} \quad (8)$$

where C_e is the conversion efficiency coefficient [parts/unit], R_g is the recovery factor [parts/unit] and depicts the ratio of energy retrieved using a particular technology to the total energy stored in the reservoir rock. T_{life} and P_f parameters are assumed system life [years] and plant factor [parts/unit], representing the gaps in the operation of the geothermal systems plant.

The recovery factor R_g was determined using the following formula (Franco & Donatini 2017):

$$R_g = \frac{\left[\left(V \cdot \left(0.5 \cdot \varphi \cdot X\right) \cdot \rho_F\right) \cdot \left(\Delta\mathrm{HR} - \Delta\mathrm{HS}\right)\right]}{\mathrm{HIP}} \quad (9)$$

where X is the degree of saturation and ΔHR – ΔHS are the fluid-rock system enthalpies.

Finally, petrophysical parameters (porosity and permeability) along with Hrec in the option utilizing water as a geothermal energy carrier were employed for classification using the generalized fuzzy c-means (gFCM) clustering method. This method is one of the classification techniques applied in machine learning (Karayiannis 1996, Zabihi & Akbarzadeh-T 2012). The classification aimed to divide the studied areas into zones of high and low geothermal potential, connected with the petrophysical characteristics of the analyzed reservoirs. The classification methodology is described in detail in the work by Topór et al. (2023).

RESULTS AND DISCUSSION

Based on the geometry of the Main Dolomite in the study area determined by the 3D structural model and the developed spatial models of porosity, permeability, and temperature, maps of the average values of these parameters characterizing the conditions of the geothermal system within the Main Dolomite were prepared, taking into account its dichotomy. Maps of the average thickness, temperature, porosity, and permeability values for limestone and dolomite horizons are presented graphically in Figures 6 (on the interleaf) ABCD and EFGH, respectively, and their statistical characteristics are depicted in Table 3.

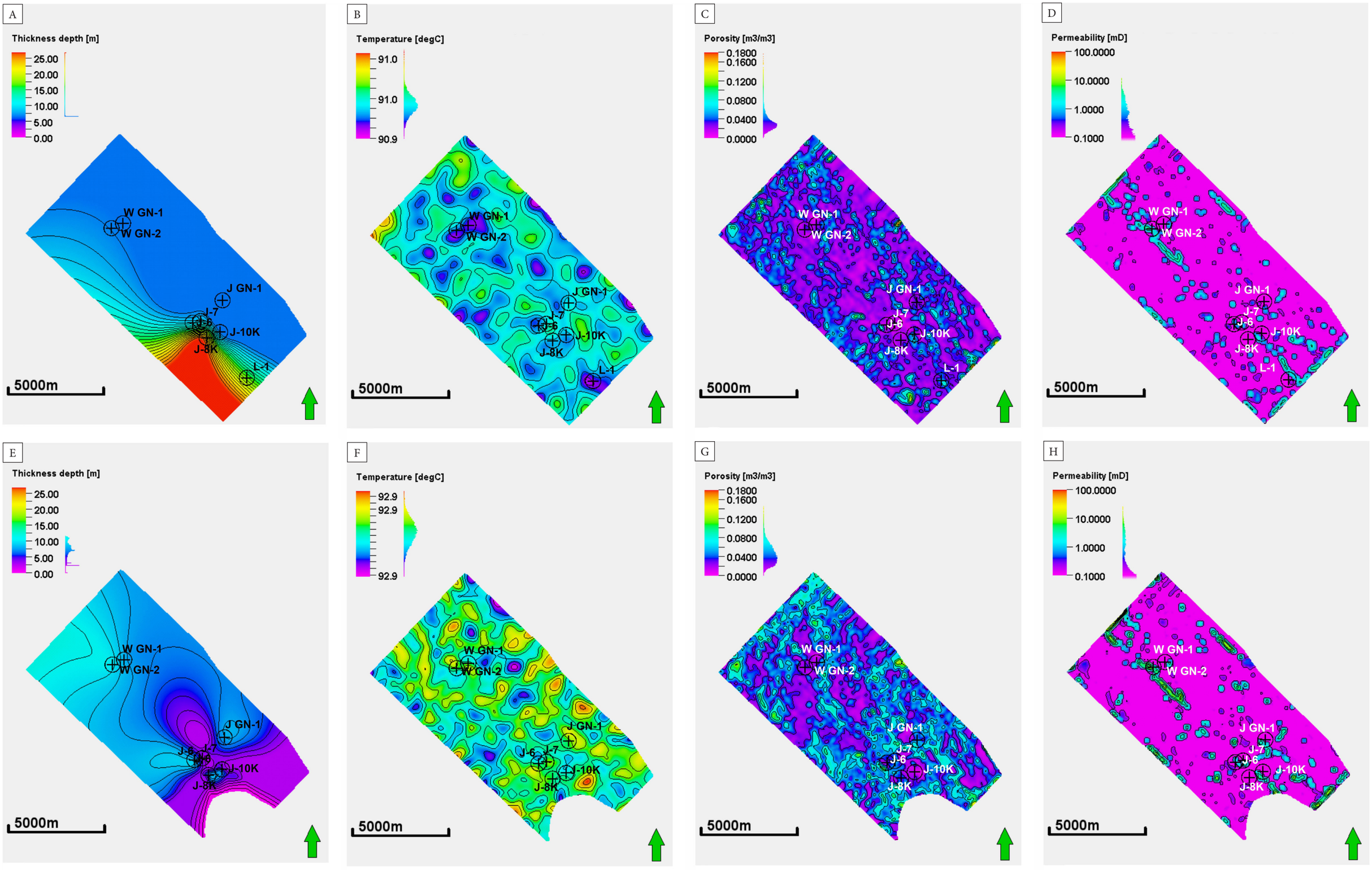

Fig. 6. *Maps depicting thickness (first column – A and E) and average temperature values (second column – B and F), porosity (third column – C and G), and permeability (fourth column – D and H) for limestone horizon (upper row, respectively A, B, C, and D) and for calcareous dolomite horizon (lower row, respectively E, F, G, and H)*

The parameters used for calculating the HIP and Hrec of a geothermal system operating for fifty years were derived from developed petrophysical and temperature 3D models, supported by well-log interpretation as well as brine and core material analysis results (unpublished reports and documentation from boreholes) and literature data (Robertson 1988, Ramalingam & Arumugam 2012, Hartlieb et al. 2015) and are listed in Tables 4–6.

Table 3
Average parameter values characterizing the distinguished in the Main Dolomite interval Ca2 limestone and dolomite lithotype

Lithotype	Thickness			Temperature			Porosity			Permeability		
	Min	Max	Mean	Min	Max	Mean	Min	Max	Mean	Min	Max	Mean geom
Limestone	6.62	26.91	9.86	89.33	92.74	90.91	0	0.177	0.032	0	11.65	0.20
Dolomite	0	11.58	6.85	92.76	93.01	92.90	0	0.146	0.045	0	26.37	0.40

Table 4
Parameters of the rock, brine, and CO_2 in supercritical form, assumed for HIP calculation

Heat capacity of rock matrix [kJ/(kg·°C)]	Heat capacity of brine [kJ/(kg·°C)]	Heat capacity of supercritical CO_2 [[kJ/(kg·°C)]	Rock density [g/cm^3]	Brine density [g/cm^3]
0.96	3.505	2.25	2.715	1.211

Table 5
Enthalpy of supercritical CO_2 assumed for the specific reservoir rock's pressure and temperature conditions

Average reservoir temperature [°C]	Average annual temperature on surface [°C] (Górecki red. 2006)	Average reservoir pressure [bar]	Enthalpy for the reservoir conditions in CO_2 system [kJ/kg]	Enthalpy for surface conditions in CO_2 system [kJ/kg]
91.62	8.9	246	–130	–310

Table 6
Assumed remaining parameters for Hrec calculation (Piris et al. 2021)

Conversion efficiency factor C_e [parts/unit]	System life factor T_{life} [years]	Plant factor P_f [parts/unit]
0.95	50	0.85

Classification using gFCM (generalized fuzzy c-means)

Petrophysical parameters such as porosity and permeability, along with Hrec, were used for classification utilizing the generalized fuzzy c-means (gFCM) clustering method. This approach allowed us to distinguish zones with varying geothermal potentials within the study area, correlating these zones directly with the inherent characteristics of the reservoirs.

The geothermal potential of the Ca2 level was investigated for two fluids as energy carriers – water and supercritical CO_2. The gFCM

clustering results for the Ca2 level were organized using Hrec_50 (water system) and ranked from the most prospective (1) to less promising (6). This potential was estimated separately for the limestone and dolomitic limestone lithotype.

Weak reservoir and filtration parameters characterize the limestone horizon. Porosity ranges from 0 to 17.7% (average 3.2%; median 2.9%), while permeability ranges from 0.007 to 11.7 mD (median 0.021 mD). The average thickness of the limestone horizon is 9.9 m. The temperature was estimated at 90.9°C (Fig. 6). The gFCM classification indicated that areas with the highest geothermal potential (highest median Hrec and HIP) occur in the southeastern part of the studied area (Fig. 7). Unfortunately, these rocks are found in a limited area and, combined with weak reservoir parameters (median for porosity Class 1 equals 6.5%) and filtration parameters (median for permeability Class 1 equals 0.196 mD), make the investigated limestone horizon less prospective. The region's lack of existing well infrastructure, which is identified as the most promising, is also a challenge. Beyond drilling new wells, effective geothermal energy extraction would require fracturing procedures, significantly increasing investment costs.

The level of calcareous dolomites (Fig. 8) locally possesses zones with better reservoir and filtration parameters compared to the limestone horizon. The average values of porosity for the entire area are 4.5% (ranging from 0 to 14.6%). Permeability varies from 0 to 26.4 mD (median 0.4 mD). Despite having better petrophysical parameters and a slightly higher temperature (92.9°C), the calcareous dolomite horizon is characterized by significantly lower thickness (average 6.9 m) compared to the limestone horizon (Fig. 7). Zones with the highest potential for geothermal energy extraction (Class 1) exhibit much greater extent, but only to a limited extent, overlap with the limestone horizon (Fig. 8). They also do not align with the existing well infrastructure. This fact significantly complicates considerations regarding the economic extraction of geothermal energy from the calcareous dolomite lithotype and the entire reservoir structure considered.

Only the areas within the more perspective dolomite horizon, marked with green polygons in Figure 9, which visualize the 3D distribution of HIP (A, B) and Hrec (C, D) for water and CO_2 as working fluids, were considered for further evaluation of geothermal energy extraction potential. In the dolomite horizon, we selected three regions situated in the northern edge (NNW) and central western (WSW) eastern (E) part of the research area, represented by rocks classified as Classes 1, 2, and 3, indicating conditions with the highest potential for geothermal energy extraction. The statistical characterization of the petrophysical and thermal conditions in those three zones is depicted in Table 7. The calculated Hrec for 50 years of a lifetime of a geothermal system for dolomite horizon in the NNW, WSW, and E part of the research area is 8.19, 3.47, 1.34, and 0.69, 0.29, 0.11 MW for water and CO_2 considered as working fluids, respectively (Table 8). The energy locked in the NNW zone constitutes nearly 21% of geothermal energy in the entire dolomite horizons in the study area.

Table 7
Statistical characteristics of petrophysical and thermal conditions in the dolomite lithotype for selected zones with the highest potential for geothermal energy extraction

Zone	Parameter											
	Thickness			Temperature			Porosity			Permeability		
	Min	Max	Mean	Min	Max	Mean	Min	Max	Mean	Min	Max	Mean
Dolomite	6.62	26.91	9.86	92.76	93.01	92.90	0.0001	0.1522	0.0447	0.0055	14.9580	0.3784
NNW	7.46	11.60	9.56	92.79	93.01	92.90	0.0059	0.1508	0.0580	0.0055	14.9580	0.4788
E	5.71	7.21	6.44	92.81	93.00	92.90	0.0084	0.1522	0.0643	0.0055	14.9580	0.4515
WSW	4.86	9.43	8.47	92.80	93.00	92.90	0.0042	0.1499	0.0562	0.0055	14.9525	0.6586

Table 8
HIP and Hrec (50 years) for water and supercritical CO_2 for selected zones with the highest potential for geothermal energy extraction

Zone	Parameter				
	Rock volume [m^3]	HIP H_2O [PJ]	HIP CO_2 [PJ]	Hrec 50 yr H_2O [MW]	Hrec 50 yr CO_2 [MW]
Dolomite horizon of the Ca2	6.16E+08	138.56	25.90	39.07	3.23
WSW	4.32E+07	9.79	1.80	3.47	0.29
E	1.45E+07	3.30	0.60	1.34	0.11
NNW	9.96E+07	22.61	4.15	8.19	0.69
Sum	1.57E+08	35.70	6.55	12.99	1.09

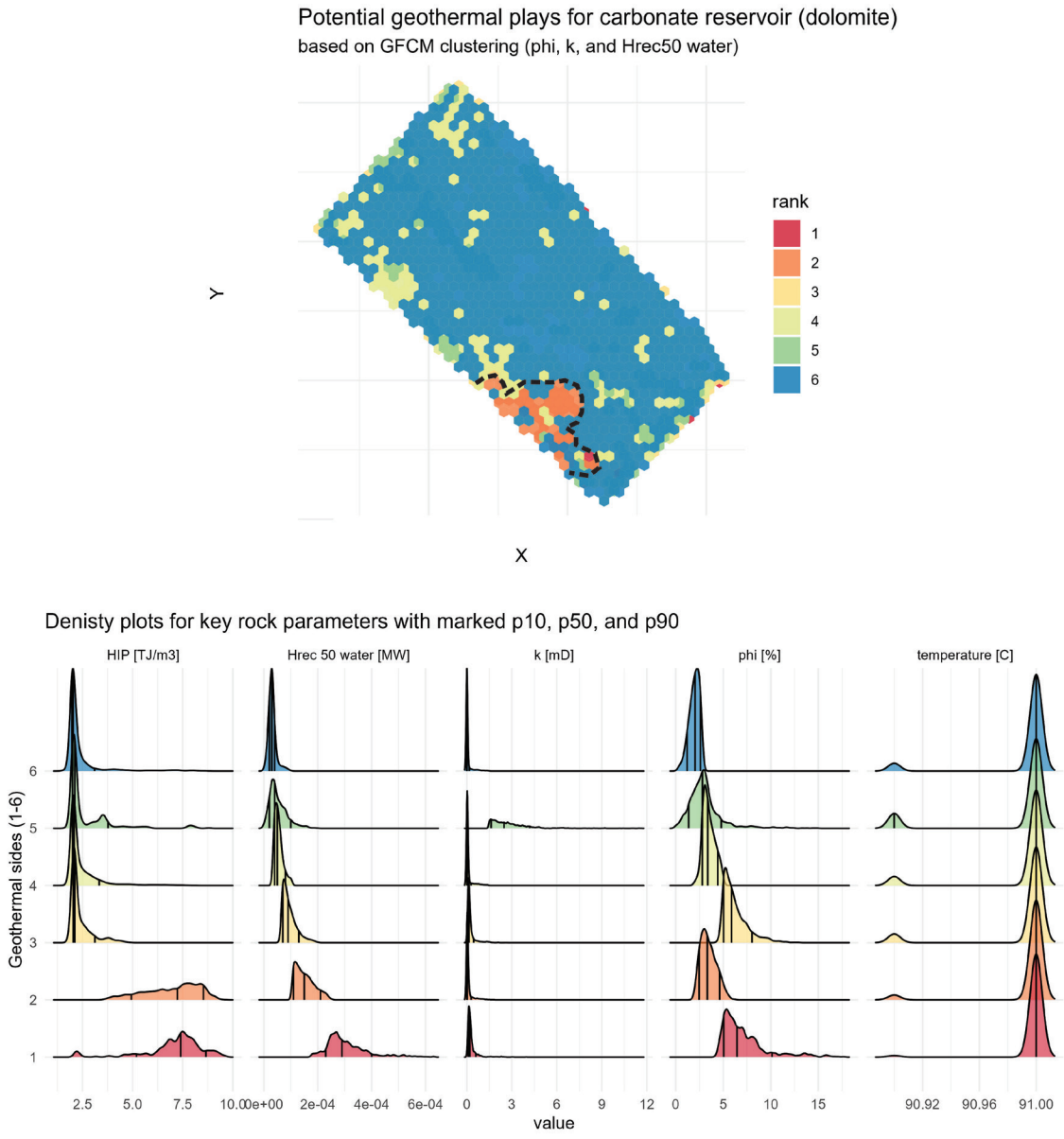

Fig. 7. *The results of the gFCM cluster analysis, along with identified areas of high and low geothermal potential and density diagrams of the main parameters for the designated Ca2 limestone lithotype*

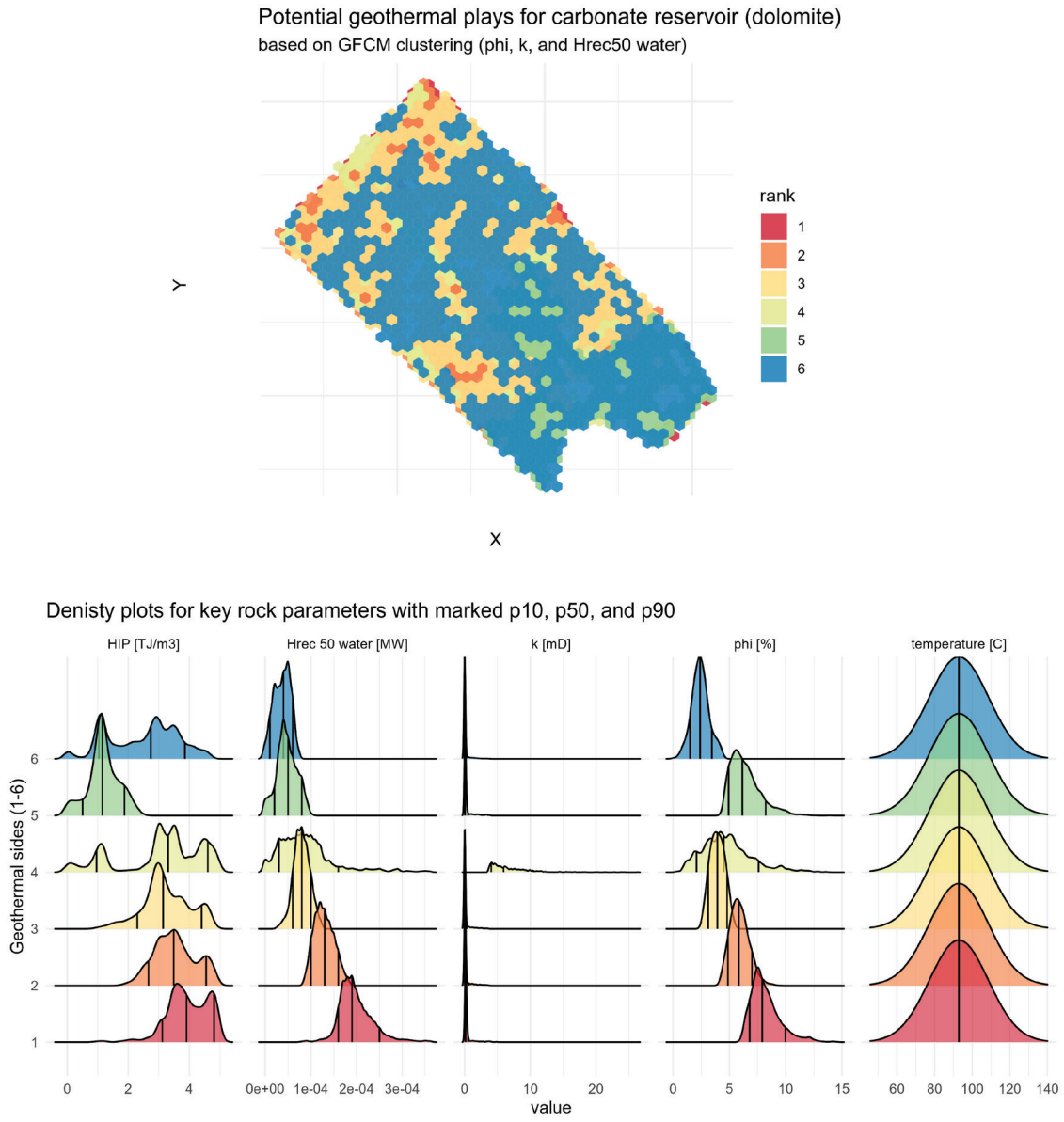

Fig. 8. *The gFCM cluster analysis results, with delineated areas of high and low geothermal potential and density diagrams of the main parameters for the specified Ca2 dolomitic limestone lithotype*

Although the CO_2 system has a lower heat capacity than water, it is now considered a promising fluid for extracting geothermal energy in EGS systems, especially for hot, dry rocks (Lei 2022). The high compressibility, expansivity, and low viscosity of CO_2 compared to water make it an attractive medium in geothermal solutions. Heat extraction using CO_2 can outperform water due to the high production rate driven by the high mobility of CO_2. Carbon dioxide consumes less pressure when it flows and can circulate automatically due to the natural thermosiphon phenomenon (Liu et al. 2019). These features can significantly offset the disadvantage of the low heat capacity of CO_2 as a heat-transmission fluid and make it an attractive medium for deep heat extraction.

The challenges of CO_2-EGS in terms of water-rock-gas interactions may consist of halite precipitation and the clogging of fractures that cause a drop in the heat extraction efficiency (Pruess 2006, Bonto et al. 2021).

Corrosion management in geothermal facilities is another critical aspect of enhancing operational efficiency and longevity, as CO_2 as a working fluid poses many issues for geothermal installations (Khasani et al. 2021).

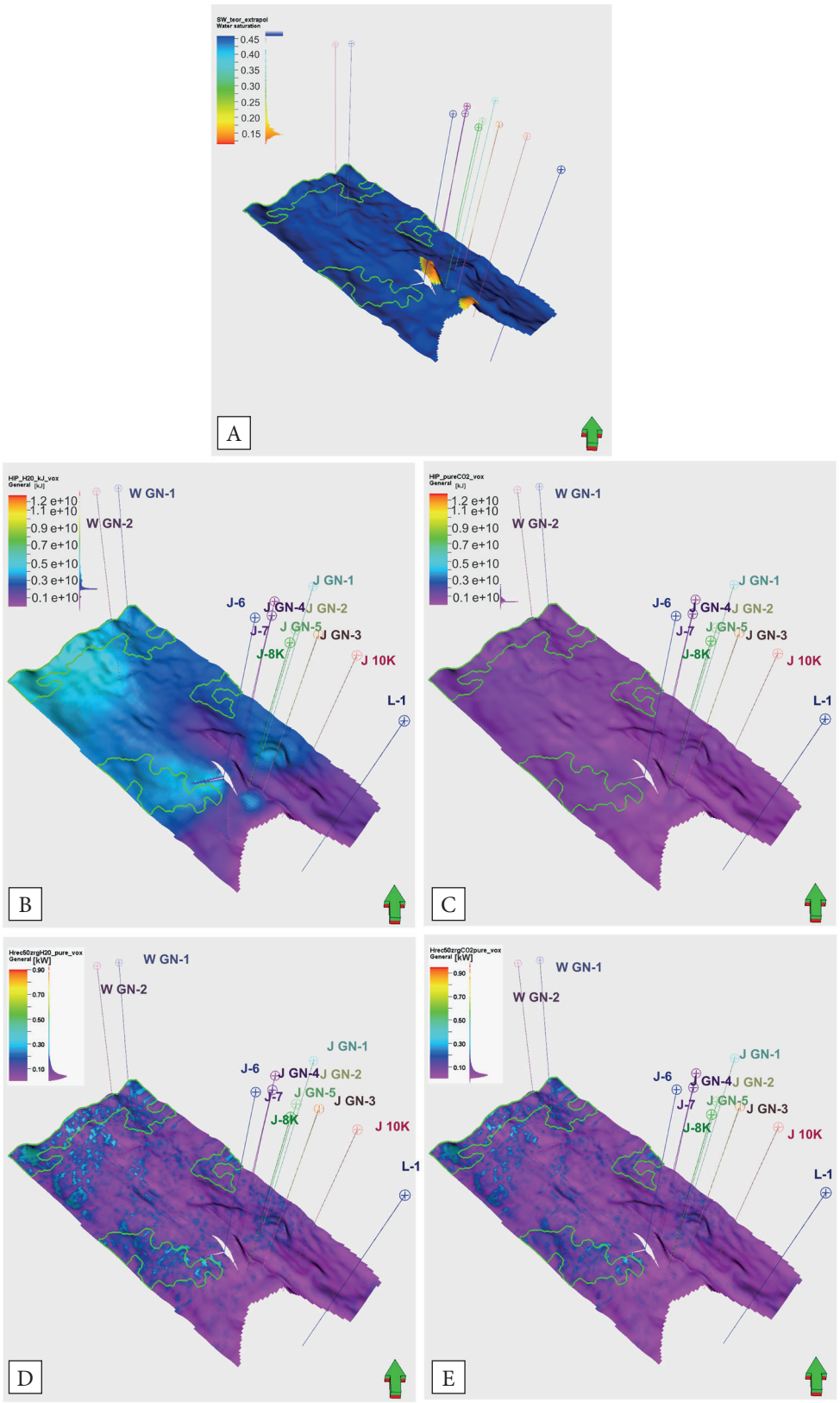

Fig. 9. *Visualization of water saturation in dolomite lithotype in the Main Dolomite (A), HIP distribution in the Main Dolomite, taking into account water (B) and CO_2 (C) as a working fluid, and the Hrec distribution considering 50-year of system lifetime for water (D) and CO_2 (E) as a working fluid*

The usage of CO_2 would also require proper examination of sealing capacity to ensure the safety of CO_2 circulation, as is done in CCS projects.

It should be emphasized that the identified hydrocarbon accumulation within the analyzed Main Dolomite horizon has not been exploited thus far; therefore, the pore space in that area is mainly saturated with hydrocarbons and irreducible water (Figs. 4, 9A).

The potential geothermal heat extraction from the hydrocarbon saturated zones would be possible after hydrocarbon production, within which the water or CO_2 as a geothermal working fluid would be injected into the reservoir formation. It could also work as a secondary hydrocarbon recovery technique. CO_2 could be considered as injection fluid in those zones due to its enhanced thermodynamic properties for geothermal energy production compared to water (Esteves et al. 2019).

SUMMARY

The assessment of geothermal potential in the Main Dolomite reservoir (Ca2) was done with the use of well log data supported 3D numerical models combined with machine learning methods to provide an outline of petrophysical (porosity and enhanced permeability) and thermal conditions in the analyzed reservoir rock and to select the most promising areas.

The conducted research led to the following conclusions:

- The reservoir rock in the Main Dolomite Ca2, characterized in terms of petrophysical and thermal conditions in the profiles of analyzed wellbores exhibits a distinct dichotomy. The upper part of the profile mainly consists of limestones and dolomitic limestones, while the lower part is composed of calcareous dolomites with anhydrite content.
- Among the two lithotypes distinctive in the Ca2 profile, the dolomites in the lower part demonstrate better petrophysical parameters and higher temperatures. These dolomites exhibit an average porosity, permeability, and temperature at mean levels of 4.5%, 0.4 mD, and 92.9°C, respectively, while having a relatively small thickness with an average value of 6.85 m.
- Based on the characteristics of the petrophysical parameters of the reservoir rock in the Main Dolomite, Ca2 was classified as an enhanced and petrothermal geothermal system.
- Due to limited flow parameters and low porosity, the Main Dolomite reservoir rock in the study area should be classified as a geothermal system requiring treatment to improve its low permeability. The classification of the reservoir rock, considering the dichotomy of the Ca2 level using the gFCM method, revealed that optimal zones within the limestones are located in the southwestern part of the analyzed area, falling into Classes 2 and 3 (shades of orange).
- Conversely, within the dolomites, the best conditions prevail in the northern edge (NNW) and, central western (WSW), and eastern (E) part of the investigated area, classified as Classes 1–3 (red and orange shades), where further calculation of geothermal energy stored in the reservoir was conducted.
- The areas with preferable conditions in the analyzed zone do not overlap with the existing wellbore network. Any potential geothermal energy production from higher potential zones would imply the need to drill additional wells.
- The calculated Hrec for 50 years of a lifetime of a geothermal system for dolomite horizon in the NNW, WSW, and E part of the research area is 8.19, 3.47, 1.34 and 0.69, 0.29, 0.11 MW for water and CO_2 considered as working fluids, respectively. The energy stored in the selected areas in dolomite horizon has a total of 12.99 and 1.09 MW, using water and CO_2 as working fluid for a 50-year system lifespan. The relatively low thickness of the limestone and dolomitic limestone horizons, their weak reservoir and filtration parameters, as well as the absence of existing infrastructure in the form of boreholes that could be easily adapted for geothermal heat extraction significantly limit the effective utilization of the investigated structure for efficient geothermal energy extraction.

This research was carried out as part of a research study funded by the Polish Ministry of Science and Higher Education, Grant No. DK-4100-51/23. The authors would like to thank the Polish Ministry of Science and Higher Education for funding this research.

REFERENCES

Archie G.E., 1942. The electrical resistivity log as an aid in determining some reservoir characteristics. *Transactions of the AIME*, 146(1), 55–62. https://doi.org/10.2118/942054-G.

Ahrens B., Lippert K. & Nehler M., 2022. *Fluid flow properties of carbonate rocks under simulated in-situ conditions: Implications for geothermal reservoir quality* [conference paper]. EGU General Assembly 2022, 23–27 May 2022, Vienna, Austria, EGU22-9858. https://doi.org/10.5194/egusphere-egu22-9858.

Bonto M., Welch M.J., Lüthje M., Andersen S.I., Veshareh M.J., Amour F., Afrough A., Mokhtari R., Hajiabadi M.R., Alizadeh M.R., Larsen C.N. & Nick H.M., 2021. Challenges and enablers for large-scale CO_2 storage in chalk formations. *Earth-Science Reviews*, 222, 103826. https://doi.org/10.1016/j.earscirev.2021.103826.

Bujakowski W. & Tomaszewska B. (red.), 2014. *Atlas wykorzystania wód termalnych do skojarzonej produkcji energii elektrycznej i cieplnej przy zastosowaniu układów binarnych w Polsce: monografia* [*Atlas of the Possible Use Geothermal Waters for Combined Production of Electricity and Heat Using Binary Systems in Poland: Monograph*]. Instytut Gospodarki Surowcami Mineralnymi i Energią Polskiej Akademii Nauk, Kraków.

CBDG (Central Geological Database), n.d. Polish Geological Institute – National Research Institute. https://baza.pgi.gov.pl/en [access: 27.03.2023].

Chomać-Pierzecka E., Sobczak A. & Soboń D., 2022. The potential and development of the geothermal energy market in Poland and the Baltic states – selected aspects. *Energies*, 15(11), 4142. https://doi.org/10.3390/en15114142.

Czekański E., Kwolek K. & Mikołajewski Z., 2010. Złoża węglowodorów w utworach cechsztyńskiego dolomitu głównego (Ca2) na bloku Gorzowa. *Przegląd Geologiczny*, 58(8), 695–703.

Esteves A.F., Santos F.M. & Magalhães Pires J.C., 2019. Carbon dioxide as geothermal working fluid: An overview. *Renewable and Sustainable Energy Reviews*, 114, 109331. https://doi.org/10.1016/j.rser.2019.109331.

Franco A. & Donatini F., 2017. Methods for the estimation of the energy stored in geothermal reservoirs. *Journal of Physics: Conference Series* [34th UIT Heat Transfer Conference 4–6 July 2016, Ferrata, Italy], 796, 012025. https://doi.org/10.1088/1742-6596/796/1/012025.

Górecki W. (red.), 2006. *Atlas zasobów geotermalnych formacji paleozoicznej na Niżu Polskim* [*Atlas of Geothermal Resources of Paleozoic Formations in the Polish Lowlands*]. Akademia Górniczo-Hutnicza im. S. Staszica, Kraków.

Górecki W., Sowiżdżał A., Hajto M. & Wachowicz-Pyzik A., 2015. Atlases of geothermal waters and energy resources in Poland. *Environmental Earth Sciences*, 74(12), 7487–7495.

GUS (Główny Urząd Statystyczny), 2023. *Gospodarka paliwowo-energetyczna w latach 2021 i 2022* [*Energy Statistics in 2021 and 2022*]. Główny Urząd Statystyczny – Statistics Poland, Urząd Statystyczny w Rzeszowie – Statistical Office in Rzeszów, Warszawa – Rzeszów. https://stat.gov.pl/en/topics/environment-energy/energy/energy-statistics-in-2021-and-2022,4,18.html [access: 22.03.2023].

Hafiz I., Albesher Z., Kellogg J. & Saeid E., 2022. Detecting the fault and fracture systems by using 3D seismic attribute – Ant-tracking algorithm. [in:] *SEG/AAPG IMAGE 2022: International Meeting for Applied Geoscience & Energy, 28 Aug – 1 Sep 2022, Houston, TX: Expanded Abstracts 2022 Technical Program*, Society of Exploration Geophysicists, Houston, 1374–1379. https://doi.org/10.1190/image2022-3738405.1.

Hajto M., 2006. Wyniki kalkulacji zasobów geotermalnych na Niżu Polskim [Calculation results of geothermal resources in the Polish Lowlands]. [in:] Górecki W. (red.), *Atlas zasobów geotermalnych formacji mezozoicznej na Niżu Polskim* [*Atlas of Geothermal Resources of Mesozoic Formations in the Polish Lowlands*], Akademia Górniczo-Hutnicza im. Stanisława Staszica, Kraków, 183–197.

Hartlieb P., Toifl M., Kuchar F., Meisels R. & Antretter T., 2015. Thermo-physical properties of selected hard rocks and their relation to microwave-assisted comminution. *Minerals Engineering*, 91, 34–41. https://doi.org/10.1016/j.mineng.2015.11.008.

Huang Y., Pang Z., Kong Y. & Watanabe N., 2021. Assessment of the high-temperature aquifer thermal energy storage (HT-ATES) potential in naturally fractured geothermal reservoirs with a stochastic discrete fracture network model. *Journal of Hydrology*, 603(part D), 127188. https://doi.org/10.1016/j.jhydrol.2021.127188.

Huang Y., Yuanzhi Ch., Ren L., Tian F., Pan S., Wang K., Wang J., Dong Y., Kong Y., Parsa M., Puppala H., Melnik O., Huang Y. & Cheng Y., 2022. Assessing the Geothermal Resource Potential of an Active Oil Field by Integrating a 3D Geological Model with the Hydro-Thermal Coupled Simulation. *Frontiers in Earth Science*, 9, 787057. https://doi.org/10.3389/feart.2021.787057.

Jarzyna J., Bała M. & Zorski T., 1999. *Metody geofizyki otworowej: pomiary i interpretacja*. Uczelniane Wydawnictwa Naukowo-Dydaktyczne AGH, Kraków.

Jaworowski K. & Mikołajewski Z., 2007. Oil- and gas-bearing sediments of the Main Dolomite (Ca2) in the Międzychód region: a depositional model and the problem of the boundary between the second and third depositional sequences in the Polish Zechstein Basin. *Przegląd Geologiczny*, 55(12/1), 1017–1024.

Jolie E., Scott S., Faulds J., Chambefort I., Axelsson G., Gutiérrez-Negrín L.C., Regenspurg S., Ziegler M., Ayling, Richter B.A. & Zemedkun M.T., 2021. Geological controls on geothermal resources for power generation. *Nature Reviews Earth & Environment*, 2, 324–339. https://doi.org/10.1038/s43017-021-00154-y.

Kaminskaite I., Wang H., Liu Z. & Li H., 2021. *Geothermal fluid flow in deep Carbonates and its impact on long-term reservoir performance: Natural systems* [conference paper]. The 82nd EAGE Annual Conference & Exhibition, October 18–21, 2021, Amsterdam, The Netherlands. https://doi.org/10.3997/2214-4609.202112851.

Karayiannis N.B., 1996. Generalized fuzzy c-means algorithms. [in:] *Proceedings of the fifth IEEE International Conference on Fuzzy Systems: FUZZ-IEEE '96; September 8-11, 1996, Hyatt Regency Hotel, New Orleans, Louisiana. Vol. 1*, IEEE, 1036–1042. https://doi.org/10.1109/FUZZY.1996.552321.

Khasani, Itoi R., Tanaka T. & Fukuda M., 2004. A numerical study on the effects of initial water saturation of a geothermal reservoir on well characteristics. *Memoirs of the Faculty of Engineering, Kyushu University*, 64(1), 1–15.

Khasani, Kusmono, Pri U. & Rachmawan B., 2021. Corrosion in geothermal facilities: Their causes, effects, mitigation, and worldwide cases. *AIP Conference Proceedings*, 2338(1), 020007. https://doi.org/10.1063/5.0066755.

Kwolek K. & Mikołajewski Z., 2007. New stratigraphic scheme for Zechstein rocks in the Pogorzela High (Foresudetic Monocline) and its significance for hydrocarbon exploration. *Przegląd Geologiczny*, 55(12/1), 1037–1047.

Lei H., 2022. Performance comparison of H_2O and CO_2 as the working fluid in coupled wellbore/reservoir systems for geothermal heat extraction. *Frontiers in Earth Science*, 10, 819778. https://doi.org/10.3389/feart.2022.819778.

Li Y. & Sun J., 2016. 3D magnetization inversion using fuzzy c-means clustering with application to geology differentiation. *Geophysics*, 81(5), J61–J78. https://doi.org/10.1190/geo2015-0636.1.

Liu Y., Wang G., Yue G., Zhang W., Zhu X., & Zhang Q., 2019. Comparison of enhanced geothermal system with water and CO_2 as working fluid: A case study in Zhacanggou, Northeastern Tibet, China. *Energy Exploration and Exploitation*, 37(2), 736–755. https://doi.org/10.1177/0144598718795492.

Mikołajewski Z. & Słowakiewicz M., 2008. Mikrofacje i diageneza utworów dolomitu głównego (Ca2) w rejonie bariery Międzychodu (Półwysep Grotowa, Polska Zachodnia). *Biuletyn Państwowego Instytutu Geologicznego*, 429, 91–97.

Moeck I.S., 2014. Catalog of geothermal play types based on geologic controls. *Renewable and Sustainable Energy Reviews*, 37, 867–882. https://doi.org/10.1016/j.rser.2014.05.032.

Muffler P. & Cataldi R., 1977. *Methods for regional assessment of geothermal resources*. U.S. Geological Survey Open-File Report 77-870, U.S. Geological Survey, Denver, Colorado. https://doi.org/10.2172/6496850.

Nathenson M., 1975. *Physical factors determining the fraction of stored energy recoverable from hydrothermal convection systems and conduction-dominated areas*. U.S. Geological Survey Open-File Report 75-525, U.S. Geological Survey. Denver, Colorado. https://doi.org/10.3133/ofr75525.

Noga B., Biernat H., Kapuściński J., Martyka P., Nowak K. & Pijewski G., 2013. Perspektywy zwiększenia pozyskiwania ciepła geotermalnego w świetle nowych inwestycji zrealizowanych na terenie Niżu Polskiego. *Technika Poszukiwań Geologicznych, Geotermia, Zrównoważony Rozwój*, 52(2/2), 75–84.

Okoroafor E.R., Smith C.M., Ochie K.I., Nwosu C.J., Gudmundsdottir H. & Aljubran M., 2022. Machine learning in subsurface geothermal energy: Two decades in review. *Geothermics*, 102, 102401. https://doi.org/10.1016/j.geothermics.2022.102401.

Peryt T.M., 2010. Ewaporaty cechsztynu PZ1-PZ3 bloku Gorzowa. *Przegląd Geologiczny*, 58(8), 689–694.

Peryt T.M. & Dyjaczyński K., 1991. An isolated carbonate bank in the Zechstein Main Dolomite Basin, Western Poland. *Journal of Petroleum Geology*, 14(4), 445–458. https://doi.org/10.1111/j.1747-5457.1991.tb01036.x.

Peryt T.M. & Mikołajewski Z., 1997. *Dokumentacja wynikowa z otworu Jarocin-8K* [unpublished].

PIG-PIB (Państwowy Instytut Geologiczny – Państwowy Instytut Badawczy), 2024. *Geotermia* [*Geothermal Resources*]. https://www.pgi.gov.pl/geotermia/przydatne/geotermia.html [access: 16.05.2024].

Pikulski L., 1997. *Dokumentacja wynikowa odwiertu Jarocin-7. Mapa strukturalna górnej części formacji dolomitu głównego na obszarze złoża ropy naftowej "Jarocin"* [unpublished].

Piris G., Herms I., Griera A., Colomer M., Arnó G. & Gomez-Rivas E., 2021. 3DHIP-Calculator – a new tool to stochastically assess deep geothermal potential using the Heat-In-Place method from voxel-based 3D geological models. *Energies*, 14(21), 7338. https://doi.org/10.3390/en14217338.

Protas A. & Wojtkowiak Z., 2000. Blok Gorzowa: Geologia dolnego cechsztynu. [in:] Biernacka J. & Skoczylas J. (red.), *Geologia i ochrona środowiska Wielkopolski: przewodnik LXXI Zjazdu Polskiego Towarzystwa Geologicznego*, Bogucki Wydawnictwo Naukowe, Poznań, 163–171.

Pruess K., 2006. Enhanced geothermal systems (EGS) using CO_2 as working fluid – A novel approach for generating renewable energy with simultaneous sequestration of carbon. Geothermics, 35(4), 351–367. https://doi.org/10.1016/j.geothermics.2006.08.002.

Ramalingam A. & Arumugam S., 2012. Experimental study on specific heat of hot brine for salt gradient solar pond application. *International Journal of ChemTech Research*, 4(3), 956–961.

Robertson E.C., 1988. *Thermal properties of rocks*. U.S. Geological Survey Open-File Report 88-441, U.S. Geological Survey, Denver, Colorado. https://doi.org/10.3133/ofr88441.

Sowiżdżał A., 2018. Geothermal energy resources in Poland – overview of the current state of knowledge. *Renewable and Sustainable Energy Reviews*, 82(3), 4020–4027. https://doi.org/10.1016/j.rser.2017.10.070.

Sowiżdżał A., Hajto M. & Górecki W., 2016. The most prospective areas for geothermal energy utilization for heating and power generation in Poland. [in:] *EGC 2016: European Geothermal Congress 2016: Strasbourg, France, 19–24 September 2016*, 1–7.

Sowiżdżał A., Starczewska M. & Papiernik B., 2022a. Future technology mix – Enhanced Geothermal System (EGS) and Carbon Capture, Utilization, and Storage (CCUS) – an overview of selected projects as an example for future investments in Poland. *Energies*, 15(10), 3505. https://doi.org/10.3390/en15103505.

Sowiżdżał A., Machowski G., Krzyżak A., Puskarczyk E., Krakowska-Madejska P. & Chmielowska A., 2022b. Petrophysical evaluation of the Lower Permian formation as a potential reservoir for CO_2 – EGS – case study from NW Poland. *Journal of Cleaner Production*, 379(part 2), 134768. https://doi.org/10.1016/j.jclepro.2022.134768.

Syukri M., Saad R., Marwan, Tarmizi, Fadhli Z. & Safitri R., 2018. Volcanic hazard implication based on magnetic signatures study of Seulawah Agam geothermal system, Indonesia. *Journal of Physics: Conference Series* [The 8th International Conference on Theoretical and Applied Physics, 20–21 September 2018, Medan, Indonesia], 1120, 012028. https://doi.org/10.1088/1742-6596/1120/1/012028.

Tagliaferri M., Gładysz P., Ungar P., Strojny M., Talluri L., Fiaschi D., Manfrida G., Andresen T. & Sowiżdżał A., 2022. Techno-economic assessment of the supercritical carbon dioxide enhanced geothermal systems. *Sustainability*, 14(24), 16580. https://doi.org/10.3390/su142416580.

Topór T., Słota-Valim M. & Kudrewicz R., 2023. Assessing the geothermal potential of selected depleted oil and gas reservoirs based on geological modeling and machine learning tools. *Energies*, 16(13), 5211. https://doi.org/10.3390/en16135211.

Wachowicz-Pyzik A., Sowiżdżał A., Maćkowski T. & Stefaniuk M., 2024. A new approach to the development of geothermal water utilization in the context of identifying and meeting the social needs of local communities: A case study from the Mogilno–Łódź Trough, Central Poland. *Sustainability*, 16(1), 37. https://doi.org/10.3390/su16010037.

Wagner R., 1994. *Stratygrafia i rozwój basenu cechsztyńskiego na Niżu Polsk*im. Prace Państwowego Instytutu Geologicznego, 146, PIG, Warszawa.

Wagner R., Dyjaczyński K., Papiernik B., Peryt T.M. & Protas A., 2000. Mapa paleogeograficzna dolomitu głównego (Ca2) w Polsce. [in:] Kotarba M.J. (red.), *Bilans i potencjał węglowodorowy dolomitu głównego basenu permskiego Polski*, Archiwum WGGiOŚ AGH, Kraków.

Zabihi M. & Akbarzadeh-T M.R., 2012. Generalized fuzzy c-means clustering with improved fuzzy partitions and shadowed sets. *ISRN Artificial Intelligence*, 2012, 92908.

Zawisza L. & Nowak J., 2012. *Metodyka określania parametrów filtracyjnych skał na podstawie kompleksowej analizy danych geofizyki otworowej*. Wydawnictwa AGH, Kraków.

Zych I., 2009. *Ropo-gazonośność dolomitu głównego na tle modelu miąższościowo-litofacjalnego cechsztynu w południowo-zachodniej części Niżu Polskiego*. Akademia Górniczo-Hutnicza im. Stanisława Staszica, Wydział Geologii, Geofizyki i Ochrony Środowiska, Katedra Surowców Energetycznych, Kraków [PhD thesis, unpublished].